Received 3 March 2007
Accepted 21 September 2007

Combination of body-fitted and embedded grids for external vehicle aerodynamics

Ralf Tilch, Ali Tabbal and Ming Zhu
ESI Group, Rungis Cedex, France
Friedhelm Decker
Volkswagen AG, Design Analysis E1, Wolfsburg, Germany, and
Rainald Löhner
Department of Computational and Data Sciences, College of Science, CFD Center, George Mason University, Fairfax, Virginia, USA

Abstract

Purpose – This paper seeks to reduce the time it takes to perform external aerodynamic simulations without compromising accuracy. At present, cleaning up CAD data sets, in particular for undercarriage parts, takes several man-weeks.

Design/methodology/approach – Body-fitted and embedded mesh techniques are combined to obtain accurate external aerodynamic solutions for realistic car geometries with minimal user intervention. The key idea is to mesh with typical body-fitted RANS grids the external shape of the vehicle, which is smooth and requires detailed physical modeling. The underhood and undercarriage are treated as embedded surfaces. The flow in this region is massively separated, requiring LES runs and isotropic grids. This makes it a suitable candidate for embedded grids.

Findings – Comparisons with body-fitted and experimental data for a typical car show that this approach can yield drag predictions with an error less than 5 percent.

Practical implications – The present approach reduces turnaround times for complete car geometries to one to two days, without compromising accuracy.

Originality/value – To the authors' knowledge, this is the first time such an approach has been tried and validated for external aerodynamics.

Keywords Flow, Finite element analysis, Automotive industry

Paper type Research paper

1. Introduction

With the advent of robust, accurate flow solvers and abundant, pervasive computer resources, the task of quickly defining a flow domain and the required boundary conditions has become a key bottleneck for numerical simulations. For external vehicle aerodynamics, the car industry at present is contemplating turnaround times of 1-2 days for arbitrary configurations. For so-called body fitted grids, the surface definition must be water-tight, and any kind of geometrical singularity, as well as small angles,

Engineering Computations: International Journal for Computer-Aided Engineering and Software
Vol. 25 No. 1, 2008
pp. 28-41

0264-4401
DOI 10.1108/02644400810841404

The authors wish to thank Volkswagen AG, Wolfsburg, Germany, for providing the data of the VW GOLF V in order to test this new approach. In particular, the authors would like to thank the "Vehicle Development CAE-Methods" department at Volkswagen, especially Dr Othmer, for the useful discussions and exchange of ideas which were the starting-point of this project.

should be avoided in order to generate a mesh of high quality. This typically presents no problems for the main "shape" of the car (the part visible to a streetside observer), but can be difficult to obtain in such a short time for the underhood and undercarriage of a typical car or truck. Experience indicates that even with sophisticated software toolkits, manual cleanup in most cases takes several days for a complete car. An alternative is to use grids that are not body-conforming, and simply "embed" the triangulations of the wetted surfaces of the structures in them. Techniques of this kind are also known as immersed, embedded, fictitious domain or Cartesian methods. The treatment of points in the vicinity of the embedded CSD triangulations or CSD bodies is modified in such a way that the required kinetic or kinematic boundary conditions are properly imposed (Clarke *et al.*, 1985; de Zeeuw and Powell, 1991; Melton *et al.*, 1993; Quirk, 1994; Karman, 1995; Pember *et al.*, 1995; Landsberg and Boris, 1997; LeVeque and Calhoun, 2001; Aftosmis *et al.*, 2000; Fadlun *et al.*, 2000; Del Pino and Pironneau, 2001; Dadone and Grossman, 2002; Peskin, 2002, Murman *et al.*, 2003; Löhner *et al.*, 2004b; Gilmanov and Sotiropoulos, 2005; Mittal and Iaccarino, 2005). At first sight, the solution of high Reynolds-number flows with grids of this type seems improper. Indeed, the portion of the surface corresponding to the external (visible) parts of a car is smooth, and the interplay of pressure gradient and viscous/advective terms is what decides if separation will occur. Therefore, for this portion of the vehicle, a highly detailed, body-fitted mesh suitable for calculations based on the Reynolds-averaged Navier stokes (RANS) equations is considered mandatory. This implies the use of highly stretched grids close to the surface in order to capture accurately boundary layers. However, for the underhood and undercarriage, many abrupt changes in curvature occur, the flow is massively separated, and a large-eddy simulation (LES) run seems sufficient. For embedded grids, this presents no problem. We are therefore in a rather fortunate position: the region where the geometry is the "dirtiest" happens to be the region where isotropic grids are sufficient, making this region a good candidate for embedded grids. The key idea is then to obtain, quickly, the external shape of the vehicle and grid it with typical body-fitted RANS grids. We remark that, this portion of the surface is typically "clean", i.e. a turnaround of 1-2 days is possible. The underhood and undercarriage, on the other hand, is then inserted into the RANS mesh generated for the external shape of the vehicle as an embedded surface. As such, it can have crossing faces (stemming, for example, from different parts of the undercarriage), and does not require elements of very high quality. A run is then conducted with the embedded mesh.

Naturally, the question arises as to how accurate the results of this combination of body-fitted and embedded-surface techniques are, and whether it can be used for daily production runs. To this end, a typical car was analyzed. The case was run with the same solver and code, exercizing the body-fitted, as well as the combined body-fitted/embedded-surface options. Pressure, velocity, as well as integrated force data were compared.

The remainder of the paper is organized as follows: Section 2 describes the overall methodology and algorithms used for external vehicle aerodynamics calculations. Section 3 details the treatment of boundary points for the embedded-mesh technique used. Section 4 shows the comparison of a purely body-fitted and a combined body-fitted/embedded run for a typical passenger car. Some conclusions and an outlook are given in Section 5.

2. Methodology

Any CFD run proceeds through the following stages:

- pre-processing;
- grid generation;
- flow solver; and
- post-processing.

In the pre-processing phase, the data and boundary conditions are acquired and defined, the desired mesh size is specified and all run-time files are prepared.

A typical vehicle data-set with underhood and undercarriage is given as 30-80 independent parts, which overlap and intersect each other in various forms. The definition of a closed and clean domain takes a considerably amount of time. Therefore, a library (quickmodeling) for the model assembly/cleaning of discrete surfaces was developed. It includes automatic tools for stitching, intersection and mesh optimisation. The intersection functionality detects splits and repatches the surfaces, and improves the intersection lines and the connected surface meshes in one step. Within this environment one is able to reduce the pre-processing time for the first closed domain to 1-3 days. An additional 3-8 days have to be added for the final mesh.

For an external vehicle flow simulation, the geometrical complexity of the underhood/undercarriage produces a complex, massively separated flow structure and reduces locally very much the need for a highly detailed, body-fitted RANS simulation. Therefore, the embedded mesh technology is applied in this region which has the consequence that the overall model preparation time can be reduced by 80-90 percent.

The highly detailed body-fitted grid is generated by the mesher. The flow solver uses the fully integrated embedded surface technology to adapt automatically the boundary-conditions, fluxes and mass-matrices for a given set of embedded surfaces and without any change in the previously generated mesh. For the applications shown here, these tasks were carried out with PRE-FLOW™ (2004), a general pre-processor that can read a variety of CAD formats, prepare the domains for CFD runs and specify the desired element size and shape in space. The necessary stitching, intersection and optimisation of the line- and surface discretisation were carried within the library quickmodeling, called by PRE-FLOW. The computational domain is then filled with tetrahedral elements of specified size by using PAM-GEN3D™ which incorporates the advancing front technique (Löhner and Parikh, 1988; Löhner, 1996; Tilch and Löhner, 2002) with a number of boundary layer gridding options. For the flow solver (PAM-FLOW™), a fractional step, projection-type finite element solver (Löhner, 2004; Löhner *et al.*, 2006; PAM-FLOW, 2004) is used. Post-processing is carried out using POST-FLOW™ (2004).

3. Embedded mesh techniques

In what follows, we denote by CSD faces the surface of the object that is embedded. We implicitly assume that this information is given by a triangulation, which typically is obtained from a CAD package via STL files.

Embedded grids are treated by imposing appropriate kinematic boundary conditions for the fluid nodes close to the embedded surfaces (Figure 1).

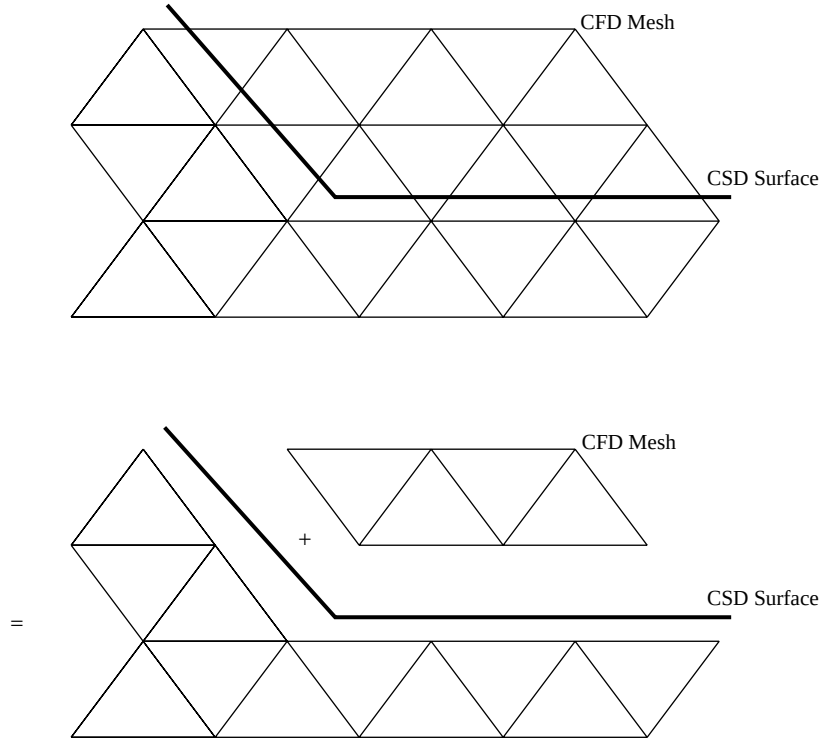

Figure 1.
Treatment of embedded surfaces

The steps required to treat embedded surfaces are:

(1) Elimination of edges crossing the embedded surface.

(2) Formation of boundary coefficients to achieve flux balance.

(3) Application of boundary conditions for the end-points of the crossed edges based on the normal of the embedded surface.

Note that the treatment of infinitely thin surfaces with fluid on both sides (e.g. membranes or shells) is straightforward. A number of fast algorithms have been developed to determine the edges crossed by the CSD faces, modify fluxes or mass-matrices close to the embedded surface, and to deactivate automatically the portions of the flow domain interior to a body (Löhner *et al.*, 2004a, b). We therefore concentrate on the treatment of boundary conditions here.

3.1 Boundary conditions

For the new boundary points belonging to cut edges, the proper PDE boundary conditions are required. For the cases considered here, these are given by an imposed velocity (Navier-stokes) or an imposed normal velocity (Euler). For limiting and higher order schemes, one may also have to impose boundary conditions on the gradients. The required surface normal and boundary velocity are obtained directly from the closest CSD face to each of the new boundary points.

These low-order boundary conditions may be improved by extrapolating the velocity from the surface with field information. The location where the flow velocity is equal to the surface velocity is the surface itself, and not the closest boundary point. As shown in Figure 2, for each boundary point the closest point on the CSD face is found. Then, two (three) neighbouring field (i.e. non-boundary) points are found and a triangular (tetrahedral) element that contains the boundary point is formed. The velocity imposed at the field point is then found by interpolation. In this way, the boundary velocity "lags" the field velocities by one timestep or inner iteration.

The normal gradients at the boundary points can be improved by considering the "most aligned" field (i.e. non-boundary) point to the line formed by the boundary point and the closest point on the CSD face (Figure 3).

4. Results for flow past A VW golf V

The case considered is shown in Figures 4-16. The physical parameters were set as follows: v_∞(33.33,0,0) m/s, $\rho = 1.2\,\mathrm{kg/m^3}$, $\mu = 1.4 \cdot 10^{-5}$ yielding a Reynolds-number of approximately $Re = 10^7$. A Smagorinsky turbulence model was used. The runs were initialized with approximately 10^3 timesteps using local timesteps. This was followed by a time-accurate run of 10^4 timesteps, integrating explicitly the advective terms in order to obtain an accurate wake. The same numeric parameters were employed for the purely body-fitted, as well as the combined body-fitted/embedded run.

The body-fitted mesh was obtained after several weeks of cleanup, and may be shown in Figure 4. Note that all the undercarriage details have been taken into account. The corresponding surface grids are shown in Figures 5 and 6. The mesh consisted of approximately 6.2 Mpts and 34.5 Mtets. Eight RANS layers were used. For the car body, the first point was $y_w = 0.455\,\mathrm{mm}$ way from the wall, and the mesh was increased by a factor of $c_i = 1.5$ between layers. No boundary layer mesh was employed for the ground. A typical result is shown in Figure 7.

For the embedded case, the starting point was given by two NASTRAN-files which came from different departments at VW. The surface which was meshed using the

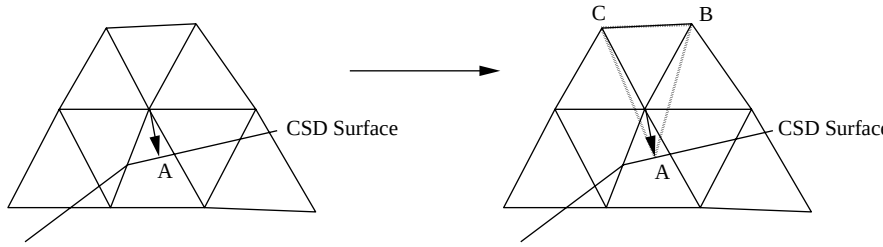

Figure 2.
Extrapolation of velocity

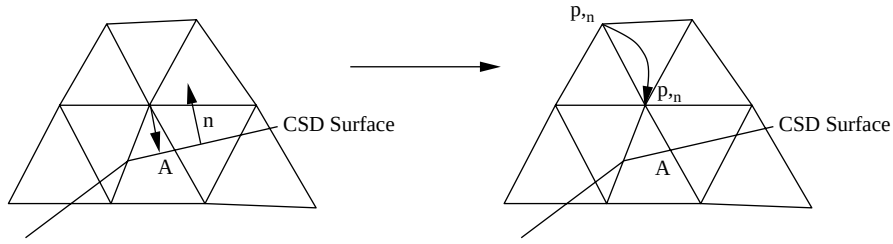

Figure 3.
Extrapolation of normal pressure gradient

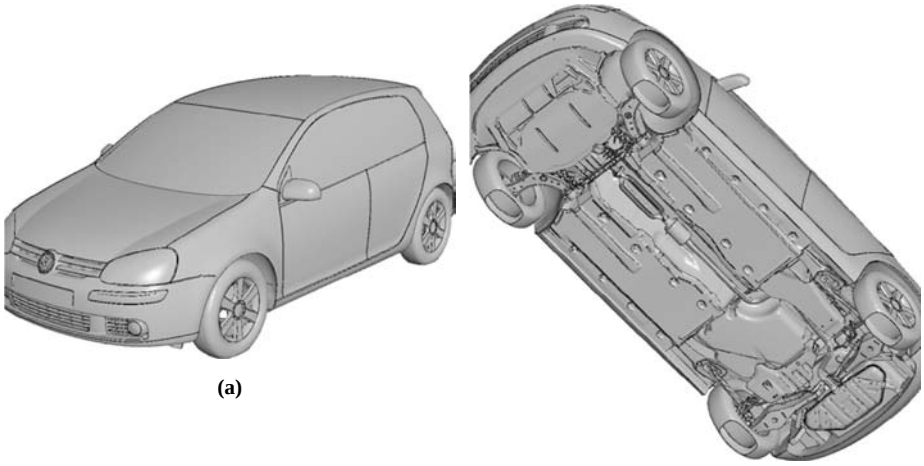

(a) **(b)**

Note: Body-fitted

Figure 4.
VW GOLF V: surface definition

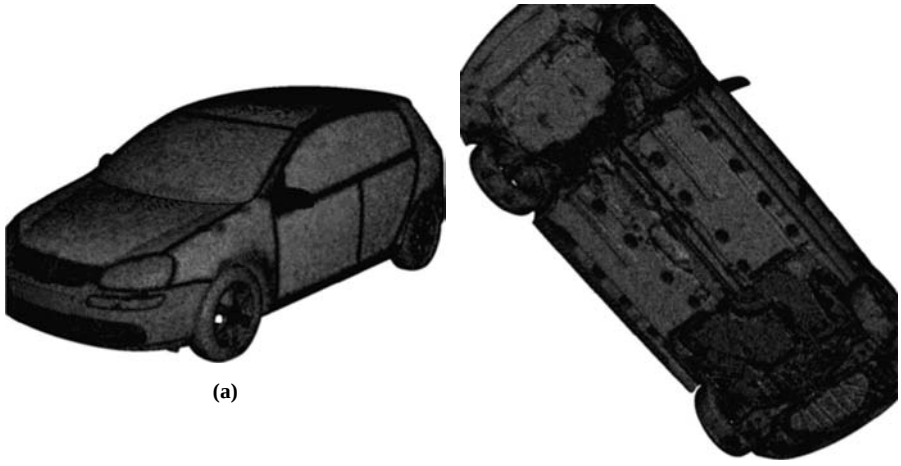

(a) **(b)**

Note: Body-fitted

Figure 5.
VW GOLF V: surface grids

body-fitted approach was supplied as four patches (one surface for the top, one for the bottom, two for the mirrors), whereas the surface which was treated with the embedded approach was given by 106 parts, most of which were single patches. The complete surface triangulation used to define the car had 1.1 Mtria. The body-fitted mesh consisted of approximately 5.68 Mpts and 32.03 Mtets. Five RANS layers were used. For the car body, the first point was $y_w = 0.758$ mm away from the wall, and the mesh was increased by a factor of $c_i = 1.5$ between layers. For the ground, the first point was

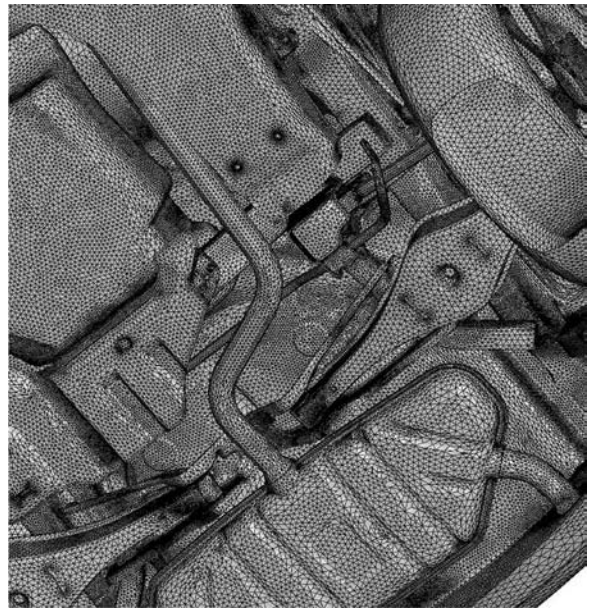

Note: Underhood detail

Figure 6.
VW GOLF V: surface grid

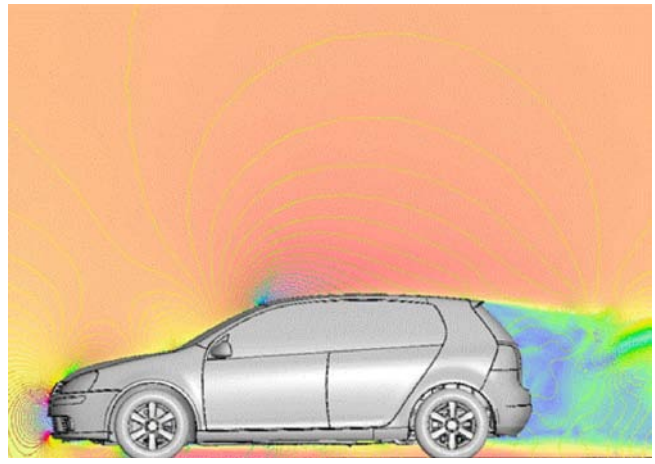

Note: Body-fitted

Figure 7.
Velocities in mid-plane

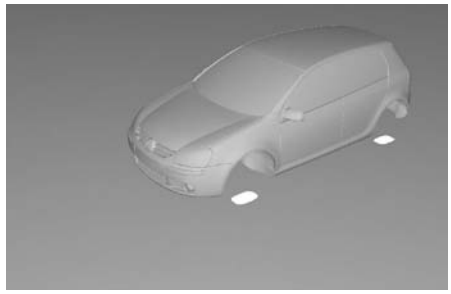

(a)

(b)

Notes: Body-fitted and embedded

Figure 8.
VW GOLF V: surface definition

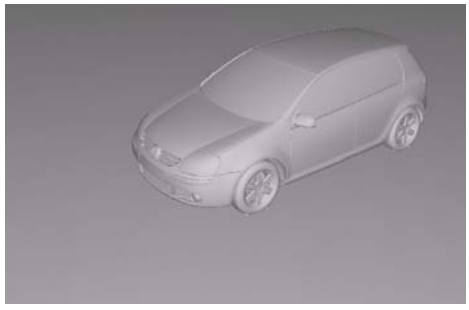

(a)

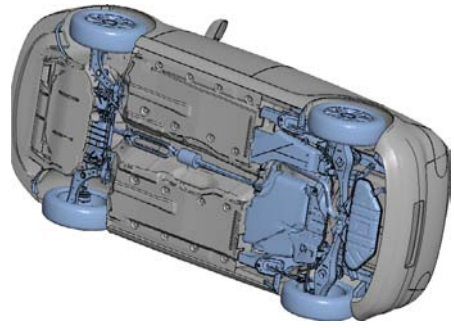

(b)

Note: Body-fitted and embedded

Figure 9.
VW GOLF V: surface definition

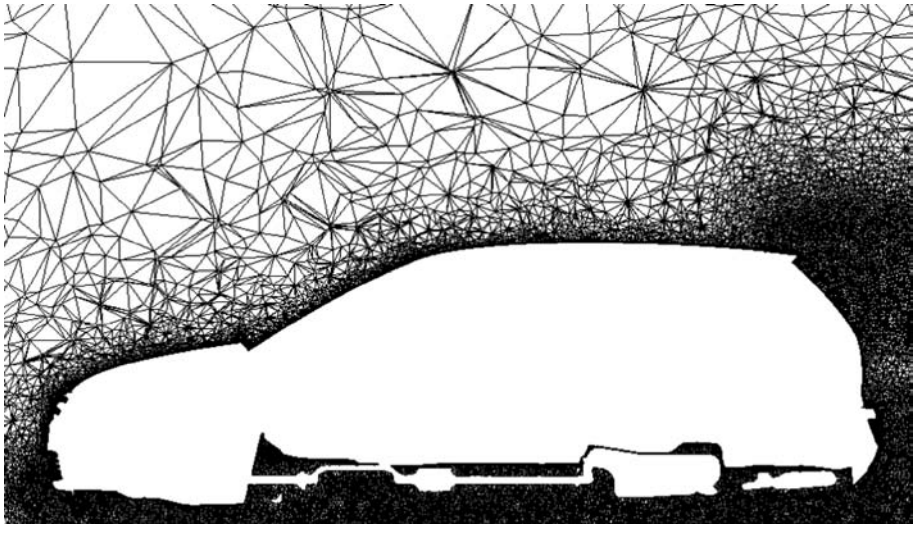

Figure 10.
Cut mesh in mid-plane

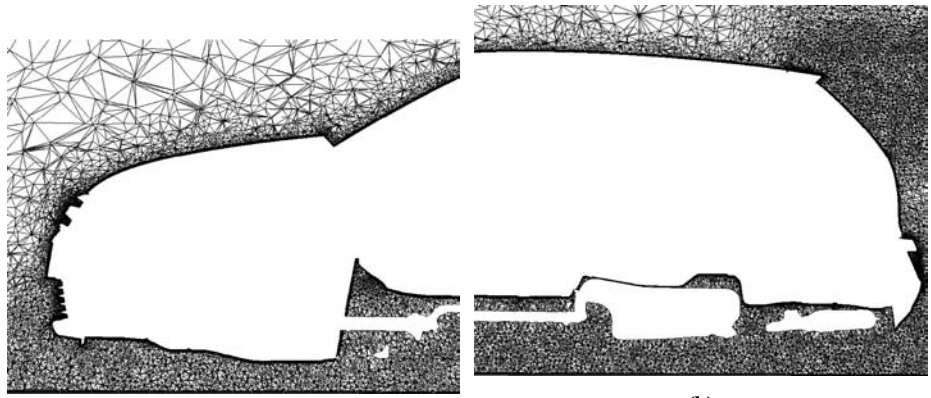

(a) (b)

Figure 11.
Cut mesh in mid-plane (detail)

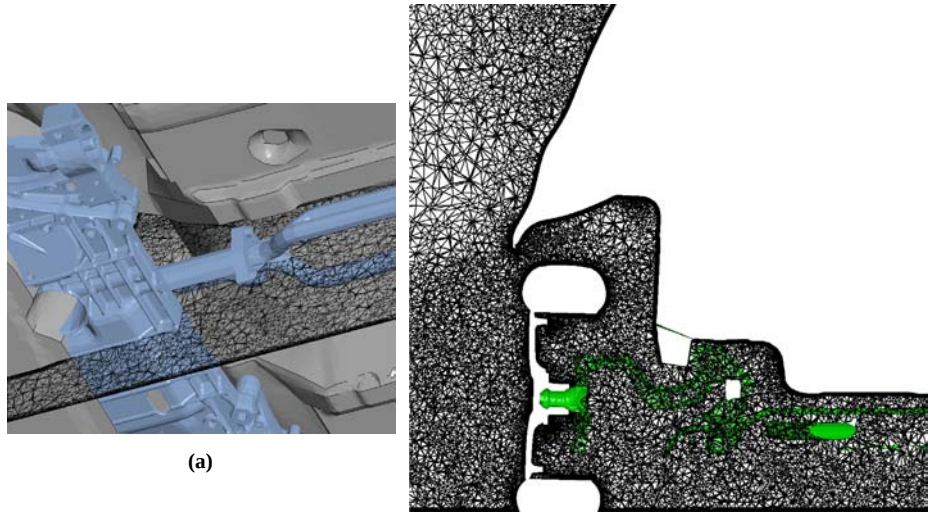

(a) (b)

Figure 12.
Undercarriage detail, cut in *x*-plane (detail)

$y_w = 0.194$ mm away from the ground, and the mesh was increased by a factor of $c_i = 1.4$ between layers. The surface of the body-fitted domain, the embedded surface, as well as the complete vehicle, are shown in Figures 8 and 9. The distribution of element size in space may be discerned from Figures 10 and 11. Note the boundary-layer mesh for the external shape, as well as the ground. A closeup of the undercarriage, together with the mesh in a cut plane and a cut in the *x*-plane are shown in Figure 12. The flowfield obtained can be shown in Figures 13-16.

The drag-coefficient obtained was $c_{\mathrm{d}} = 0.309$, based on a reference velocity of $v_\infty = 33.33$ m/s and an area of $A = 2.2\,\mathrm{m}^2$. Experiments conducted at VW measured a drag-coefficient of $c_{\mathrm{d}} = 0.330$. However, the windtunnel model exhibited an open grille.

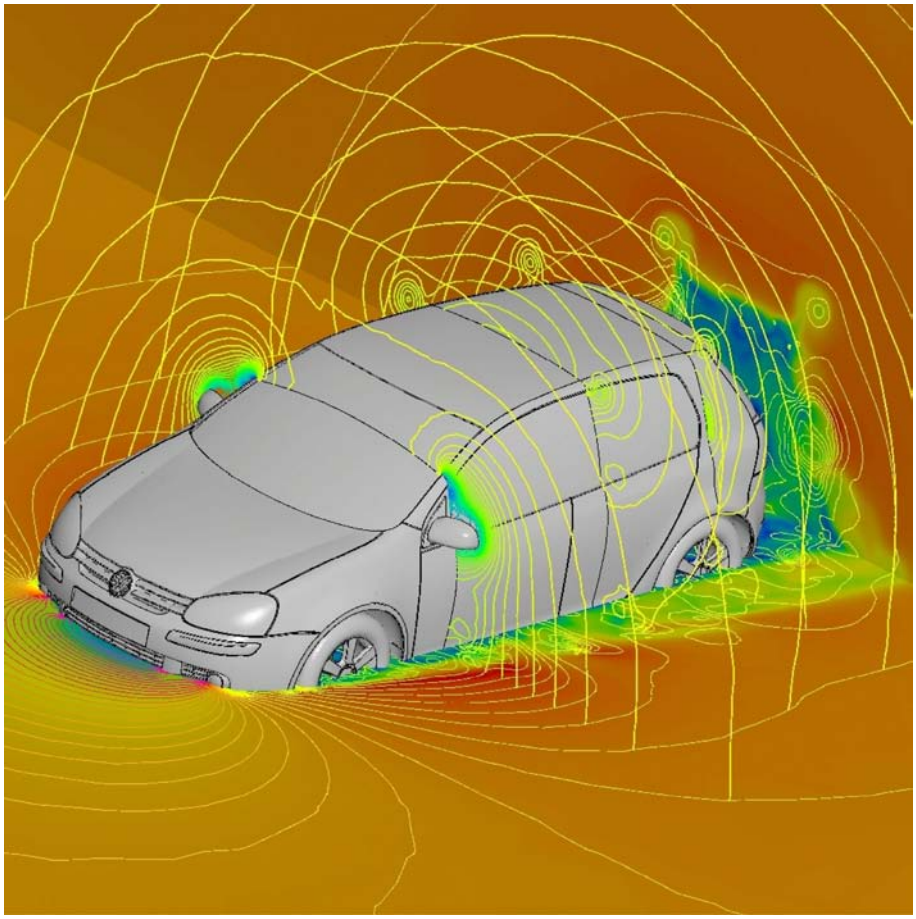

Figure 13.
Pressure (contours) on y-plane and x-planes, velocity (shaded) in y-plane and back x-plane

From past experience, one can infer that performing the experiment with a closed front, as was done for the present run, would reduce the c_d by 5-10 percent in comparison with an open grille. At VW, the estimated value for the closed grille case was $c_d = 0.305$. The purely body-fitted CFD run with the same code yielded a drag-coefficient of $c_d = 0.320$. Overall, this leads us to conclude that with the present approach results within 5 percent of experimental values can be obtained, not bad considering the reduction in set-up times, and well within a range to make them of interest for designers. Moreover, as experience with this approach accumulates, we expect to be able to obtain even better results.

5. Conclusions and outlook

Body-fitted and embedded mesh techniques were combined to obtain accurate external-aerodynamic solutions for realistic car geometries with minimal user intervention. The key idea is to mesh with typical body-fitted RANS grids the

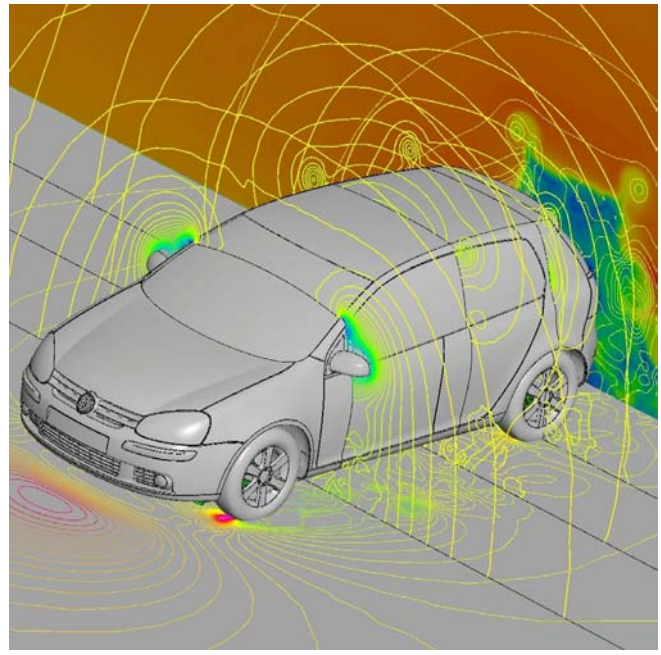

Figure 14.
Pressure (contours) on ground and *x*-planes, velocity (shaded) in back *x*-plane

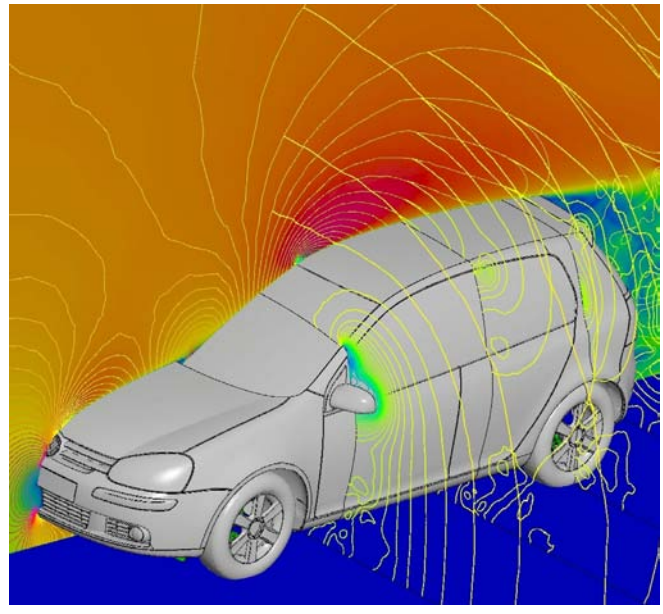

Figure 15.
Pressure (contours) and velocity (shaded) in mid-plane, pressure (contours) in *x*-planes

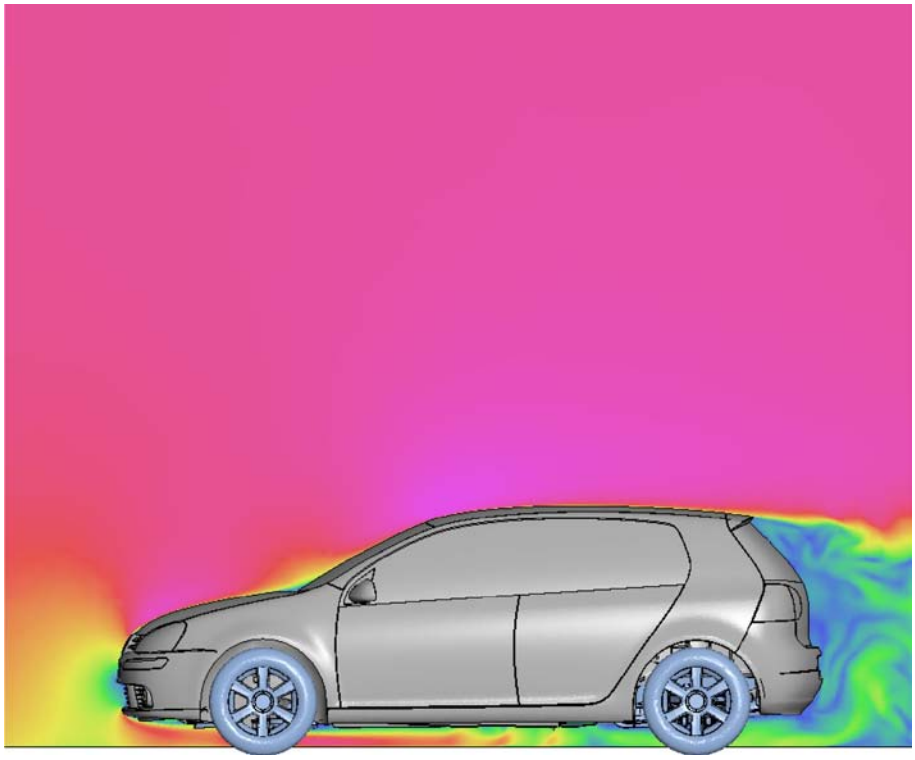

Notes: Body-fitted and embedded

Figure 16.
Velocities in mid-plane

external shape of the vehicle, which is smooth and requires detailed physical modeling. The underhood and undercarriage are treated as embedded surfaces. The flow in this region is massively separated, requiring LES runs and isotropic grids. This makes it a suitable candidate for embedded grids.

Comparisons with body-fitted and experimental data show that, this approach can yield drag predictions with an error less than 5 percent.

The great advantage seen in the present approach is that turnaround times for complete car geometries can be lowered to one to two days without compromising accuracy.

References

Aftosmis, M.J., Berger, M.J. and Adomavicius, G. (2000), "A parallel multilevel method for adaptively refined Cartesian grids with embedded boundaries", AIAA-00-0808.

Clarke, D.K., Hassan, H.A. and Salas, M.D. (1985), "Euler calculations for multielement airfoils using Cartesian grids", AIAA-85-0291.

Dadone, A. and Grossman, B. (2002), "An immersed boundary methodology for inviscid flows on Cartesian grids", AIAA-02-1059.

de Zeeuw, D. and Powell, K. (1991), "An adaptively-refined Cartesian mesh solver for the Euler equations", AIAA-91-1542.

Del Pino, S. and Pironneau, O. (2001), "Fictitious domain methods and freefem3d", *Proceedings of ECCOMAS CFD Conference, Swansea, Wales*.

Fadlun, E.A., Verzicco, R., Orlando, P. and Moud-Yusof, J. (2000), "Combined immersed-boundary finite-difference methods for three-dimensional complex flow simulations", *J. Comp. Phys.*, Vol. 161, pp. 33-60.

Gilmanov, A. and Sotiropoulos, F. (2005), "A hybrid Cartesian/immersed boundary method for simulating flows with 3-D, geometrically complex moving bodies", *J. Comp. Phys.*, Vol. 207 No. 2, pp. 457-92.

Karman, S.L. (1995), "SPLITFLOW: a 3-D unstructured Cartesian/prismatic grid CFD code for complex geometries", AIAA-95-0343.

Landsberg, A.M. and Boris, J.P. (1997), "The virtual cell embedding method: a simple approach for gridding complex geometries", AIAA-97-1982.

LeVeque, R.J. and Calhoun, D. (2001), "Cartesian grid methods for fluid flow in complex geometries", in Fauci, L.J. and Gueron, S. (Eds), *Computational Modeling in Biological Fluid Dynamics*, Vol. 124, Springer-Verlag, New York, NY, pp. 117-43, IMA Volumes in Mathematics and its Applications.

Löhner, R. (1996), "Extensions and improvements of the advancing front grid generation technique", *Comm. Num. Meth. Eng.*, Vol. 12, pp. 683-702.

Löhner, R. (2004), "Multistage explicit advective prediction for projection-type incompressible flow solvers", *J. Comp. Phys.*, Vol. 195, pp. 143-52.

Löhner, R. and Parikh, P. (1988), "Three-dimensional grid generation by the advancing front method", *Int. J. Num. Meth. Fluids*, Vol. 8, pp. 1135-49.

Löhner, R., Baum, J.D. and Mestreau, E.L. (2004a), "Advances in adaptive embedded unstructured grid methods", AIAA-04-0083.

Löhner, R., Baum, J.D., Mestreau, E.L., Sharov, D., Charman, C. and Pelessone, D. (2004b), "Adaptive embedded unstructured grid methods", *Int. J. Num. Meth. Eng.*, Vol. 60, pp. 641-60.

Löhner, R., Yang, C., Cebral, J.R., Camelli, F., Soto, O. and Waltz, J. (2006), "Improving the speed and accuracy of projection-type incompressible flow solvers", *Comp. Meth. Appl. Mech. Eng.*, Vol. 195 Nos 23/24, pp. 3087-109.

Melton, J.E., Berger, M.J. and Aftosmis, M.J. (1993), "3-D applications of a Cartesian grid Euler method", AIAA-93-0853-CP.

Mittal, R. and Iaccarino, G. (2005), "Immersed boundary methods", *Annu. Rev. Fluid Mech.*, Vol. 37, pp. 239-61.

Murman, S.M., Aftosmis, M.J. and Berger, M.J. (2003), "Implicit approaches for moving boundaries in a 3-D Cartesian method", AIAA-03-1119.

PAM-FLOW™ (2004), *Reference Manual©(PDF) & User Manual©(PDF)*, ESI Group, Rungis Cedex.

Pember, R.B., Bell, J.B., Colella, P., Crutchfield, W.Y. and Welcome, M.L. (1995), "An adaptive Cartesian grid method for unsteady compressible flow in irregular regions", *J. Comp. Phys.*, Vol. 120, p. 278.

Peskin, C.S. (2002), "The immersed boundary method", *Acta Numerica*, Vol. 11, pp. 479-517.

POST-FLOW™ (2004), *Reference Manual©(PDF), ESI Group*, ESI Group, Rungis Cedex.

PRE-FLOW™ (2004), *Reference Manual©(PDF), ESI Group*, ESI Group, Rungis Cedex.

Quirk, J.J. (1994), "A Cartesian grid approach with hierarchical refinement for compressible flows", NASA CR-194938, ICASE Report No. 94-51.

Tilch, R. and Löhner, R. (2002), "Advances in discrete surface grid generation: towards a reliable industrial tool for CFD", AIAA-02-0862.

Further reading

Mohd-Yusof, J. (1997), "Combined immersed-boundary/b-spline methods for simulations of flow in complex geometries", *CTR Annual Research Briefs*, NASA Ames Research Center/ Stanford University, Stanford, CA, pp. 317-27.

Corresponding author

Rainald Löhner can be contacted at: rlohner@gmu.edu